THE ASTROPHYSICAL JOURNAL, 516:647–659, 1999 May 10

IS THE BUTCHER-OEMLER EFFECT A FUNCTION OF THE CLUSTER REDSHIFT?

S. ANDREON
Osservatorio Astronomico di Capodimonte, via Moiariello 16, 80131 Napoli, Italy; andreon@na.astro.it
AND
S. ETTORI
Institute of Astronomy, Madingley Road, Cambridge CB3 0HA, England, UK; settori@ast.cam.ac.uk
Received 1998 May 29; accepted 1998 December 18

ABSTRACT

Using PSPC *ROSAT* data, we measure the X-ray surface brightness profiles, size, and luminosity of the Butcher-Oemler (BO) sample of clusters of galaxies. The cluster X-ray size, as measured by the Petrosian $r_{\eta=2}$ radius, does not change with redshift and is independent of X-ray luminosity. On the other hand, the X-ray luminosity increases with redshift. Considering that fair samples show no evolution, or negative luminosity evolution, we conclude that the BO sample is not formed from the same class of objects observed at different look-back times. This is in conflict with the usual interpretation of the Butcher-Oemler as an evolutionary (or redshift dependent) effect, based on the assumption that we are comparing the same class of objects at different redshifts. Other trends present in the BO sample reflect selection criteria rather than differences in look-back time, as independently confirmed by the fact that trends lose strength when we enlarge the sample with an X-ray–selected sample of clusters. The variety of optical sizes and shapes of the clusters in the Butcher-Oemler sample and the Malmquist-like bias are the reasons for these selection effects that mimic the trends usually interpreted as changes due to evolution.

Subject headings: galaxies: evolution — galaxies: photometry — X-rays: galaxies

1. INTRODUCTION

Galaxies in distant ($z \sim 0.4$) clusters differ from those in the nearby systems (see, e.g., Butcher & Oemler 1984; Dressler & Gunn 1992). There is a blueing of galaxy color with redshift, also known as the Butcher-Oemler effect (hereafter BO effect; Butcher & Oemler 1977, 1984). At $z \sim 0.4$ there is a population of almost normal late-type galaxies that by the present epoch has disappeared, faded, or been disrupted (Dressler et al. 1997). Distant clusters contain galaxies with disturbed morphologies and peculiar spectra. The occurrence of these peculiarities varies from cluster to cluster and, on average, increases with redshift. In general, the change of galaxy properties is explained as the effect of some kind of evolution.

Oemler, Dressler, & Butcher (1997) proposed a physical reason to explain why most of the clusters showing a BO effect are at high redshift and almost none at the present epoch: clusters at $z \sim 0.4$ are much more exceptional objects than present-day clusters, and they are observed in the act of growing by merger of smaller clumps, in agreement with a hierarchical growth of structures as described, for example, by Kauffmann (1995). Furthermore, this scenario permits the existence of dynamically young local clusters, such as the spiral rich Abell 1367 and 2151 clusters, and evolved clusters at high redshift, such as Cl 0024+16. In the Oemler et al. (1997) interpretation of the BO effect, clusters at higher redshift are dynamically younger, on average, than the nearby ones, because we are looking at the epoch of an enhanced cluster formation.

Allington-Smith et al. (1993) showed that galaxies in groups do not evolve (except passively) and suggest that the BO effect should be interpreted as an evidence of the important role played by the cluster environment: evolution is strong in clusters and negligible in groups. However, this idea has been questioned: Rakos & Schombert (1995) show that it is difficult to fade the majority of the cluster population at $z \sim 0.7$ to make their blue population as scarce as in present-day clusters. Andreon, Davoust, & Heim (1997) and Ellis et al. (1997) show that cluster elliptical and lenticular galaxies are old galaxies already at $z \sim 0.4$ and that the majority of them cannot be the end product of the blue galaxy population. Recently, this result has been extended with clusters up to $z \sim 0.9$ (Stanford, Eisenhardt, & Dickinson 1998).

Andreon et al. (1997) have made a detailed comparison of the properties of galaxies in the nearby Coma Cluster and the distant cluster Cl 0939+47. They found that the spiral population of these two clusters appears too different in spatial, color, and surface brightness distributions to be the same galaxy population observed at two different epochs. The Coma Cluster is therefore unlikely to be representative of the end of the evolutionary path of Cl 0939+47.

In order to quantify the effect of evolution on the properties of a given class of objects, it is required that the observed class is the same at different times. In the case of the evolution of galaxies in clusters, it is necessary that the high-redshift clusters studied are the ancestors of the investigated present-day clusters.

The goal of this paper is to test whether the distant and nearby clusters of the BO sample are really the same population seen at different epochs or two different populations; in other words, we want to check whether we are comparing unripe apples to ripe oranges in understanding how fruit ripens! We achieve this goal by means of the X-ray properties of the clusters of galaxies, whose evolution is known.

The paper is organized as follows: in § 2, we present our sample of clusters. In § 3, we discuss the X-ray analysis of their images. The observed trends and their relevance to the BO effect are presented in §§ 4 and 5, respectively. In § 6, we summarize our main results.

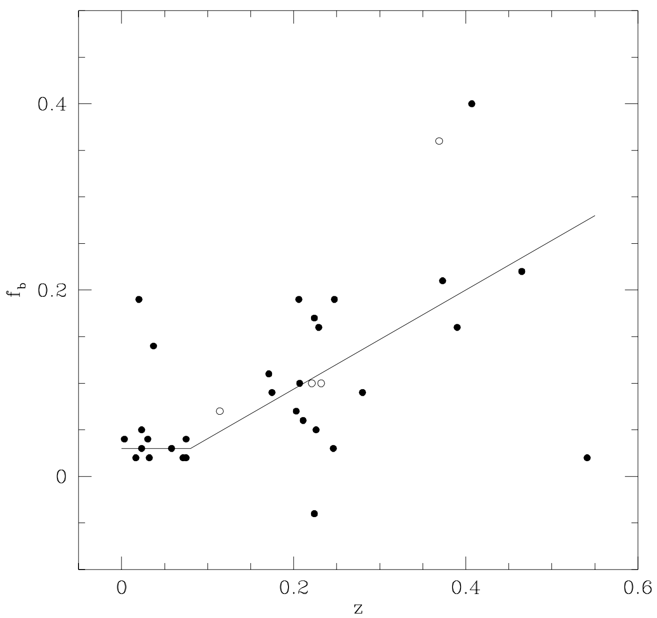

FIG. 1.—Blue fraction as a function of z for the whole sample (which is the BO sample with the addition of the cluster Cl 0939+47). Filled and open dots mark clusters with and without X-ray data, respectively. The spline is the Butcher & Oemler (1984) eye fit to the data.

In the following analysis, we adopt $H_0 = 50$ km s^{-1} Mpc^{-1} and $q_0 = 0.5$. The conversion to the physical dimension is done through the equation (Sandage 1988)

$$r(\mathrm{kpc}) = 2.91 \times 10^3 \times \theta \, \frac{z + 1 - \sqrt{z+1}}{H_0(1+z)^2} \,, \qquad (1)$$

where θ is the angular radius in arcseconds.

2. OUR SAMPLE: THE BUTCHER 12 & OEMLER (1984) SAMPLE

The clusters most frequently compared for measuring the BO effect are listed in Butcher & Oemler (1984). This list is the master list for many studies (e.g., Dressler & Gunn 1992; Oemler et al. 1997; half of the sample by Smail et al. 1997; Dressler et al. 1997 is drawn from the BO sample, etc.).

Our sample is made from the BO sample plus Cl 0939+47, a cluster at $z \sim 0.4$ that is frequently studied in the context of the BO effect. This sample, which consists of 33(+1) clusters, is not complete in any sense (in cluster richness, in z, etc.). Figure 1 reproduces Figure 3 in Butcher & Oemler (1984), with the addition of Cl 0939+47. The BO effect is evident from the increase of the fraction of blue galaxies with redshift.

We have X-ray data for 30 of the 34 clusters. Position Sensitive Proportional Counter (PSPC) images are available for 25 of these. We call this subsample the "HQ" (high quality) sample.

Five more clusters, as well as many of the clusters observed by *ROSAT*, have been observed with previous X-ray missions. We use these old data when necessary.

Table 1 presents the whole sample in order of increasing redshift. The columns list (1) the cluster name; (2) the cluster redshift; (3) the radius r_{30}, which contains 30% of the whole cluster population; (4) the number of galaxies N_{30} inside such a radius; and (5) the cluster blue fraction f_b (from Butcher & Oemler 1984). Columns (6) and (7) list the Galactic H I column (from Stark et al. 1992) toward the cluster direction and the cluster richness (from the Abell, Corwin, & Olowin [1989, hereafter ACO] catalog). In column (8), clusters with X-ray flux data collected from the literature and clusters belonging to the HQ sample are indicated by single and double plus signs, respectively. We update the richness classification of the Cl 0939+47 (Abell 851) and Abell 370 clusters, and we attribute a richness to Cl 0024+16 by adopting the more accurate values listed in Oemler et al. (1997). Cl 0016+16 is twice as rich as Coma (Koo 1981). The ACO richness, according to its definition, is the background-corrected number of galaxies within 3 Mpc from the cluster center having luminosity in the range M_3 and $M_3 + 2$, where M_3 is the magnitude of the third brightest cluster galaxy.

3. DATA ANALYSIS

3.1. *Data Reduction*

PSPC images in the hard band 0.5–2 keV with 15″ pixel size have been extracted from the public archive at the Max-Planck-Institut für extraterrestrische Physik (MPE) or at the Goddard Space Flight Center (according to their availability). Table 2 lists X-ray–related quantities. We correct our images for exposure variation and telescope vignetting using the distributed exposure maps. All pixels contaminated by other objects or occulted by ribs have been flagged and excluded from the following analysis.

In order to measure the X-ray radial profiles, brightnesses are computed in elliptical annuli of semimajor axis increasing in geometrical progression of base $\sqrt{2}$ in order to take the signal-to-noise ratio (S/N) approximatively constant along the radius.

Ellipticity, position angle (P.A.), and center for the cluster emission have been derived paying attention to the observational data available for distant clusters. For example, we keep fixed the center, even if isophotes' center moves, because in distant clusters we seldom have data of good enough quality to measure the displacement of the center of the various isophotes.

When the data are not good enough to estimate the ellipticity or the position angle, we adopt circular apertures.

The details of the data reduction are as follows:

1. The equivalent radius of each ellipse is that of a circle of the same area, i.e., $r = \sqrt{ab}$, where a, b are the major and minor axes of the ellipse.
2. The axis lengths of an elliptical annulus of finite width are halfway from the internal and external edges.
3. The brightness in an annulus is computed as the ratio of the intensity measured in unflagged pixels to their total area.
4. We assume that flagged pixels have the same brightness as unflagged ones in the same annulus. The flux inside an ellipse is the sum, over the internal annulus, of the product of the brightness computed in each annulus and the total area of the annulus (calculated including the flagged pixels).

Before we proceed further in the data analysis, we need to verify two assumptions: the computed profiles are independent (i) of the exact choice of the flagged pixels and (ii) of the ellipticity and P.A. chosen for the integration. We apply two different flag schemes to the same image of Abell 2218:

TABLE 1

THE BO SAMPLE

Name (1)	z (2)	r_{30} (arcmin) (3)	N_{30} (4)	f_b (5)	N_H (10^{20} atoms cm^{-2}) (6)	R (7)	X-Ray? (8)
Virgo	0.0033	120	21	0.04	...	...	+
Abell 262	0.0164	27	22	0.02	5.3	0	++
Abell 1367	0.02	25	20	0.4	2.1	2	++
Abell 400	0.0232	17	30	0.05	8.7	1	++
Abell 1656	0.0232	22	94	0.03	0.91	2	++
Abell 2199	0.0305	18	94	0.04	0.88	2	++
Abell 2634	0.0322	30	60	0.02	4.9	1	++
Abell 2151	0.0371	14	29	0.14	3.4	1	++
Abell 2256	0.0581	11	116	0.03	4.2	2	++
Abell 1904	0.0714	9.4	68	0.02	1.8	2	++
Abell 401	0.0748	10.7	92	0.02	1.1	2	++
Abell 2670	0.0749	4.9	51	0.04	2.7	3	++
Cl 0004.8−34	0.114	5.9	60	0.07	...	...	...
Abell 2218	0.171	5.8	114	0.11	3.3	4	++
Abell 1689	0.1747	5.8	124	0.09	1.8	4	++
Abell 520	0.203	4.5	126	0.07	7.6	3	++
Abell 963	0.206	3.6	88	0.19	1.4	0	++
Abell 223	0.207	3.2	67	0.10	1.9	3	++
Abell 222	0.211	1.6	45	0.06	1.8	3	++
Abell 1963	0.221	1.5	38	0.10	...	2	...
Abell 1942	0.224	2.8	57	0.17	...	3	+
Abell 2397	0.224	2.0	23	−0.04	5.6	3	++
Abell 777	0.226	1.4	15	0.05	1.9	4	++
Abell 2111	0.229	4.1	155	0.16	1.9	3	++
Abell 1961	0.232	3.4	88	0.10	...	3	...
Abell 2645	0.246	1.4	35	0.03	...	4	+
Abell 2125	0.2472	2.3	62	0.19	2.9	4	++
Abell 1758	0.280	2.4	91	0.09	1.1	3	++
Cl 1446+26	0.369	0.9	42	0.36	...	...	...
Abell 370	0.373	2.2	107	0.21	...	2	+
Cl 0024+16	0.39	1.1	87	0.16	4.2	2	++
Cl 0939+47	0.407	1.0	...	0.4	1.3	5	++
3C295	0.465	1.0	45	0.22	...	...	+
Cl 0016+16	0.541	1.0	65	0.02	4.1	4	++

NOTE.—In the last column, clusters with X-ray flux data collected from the literature and clusters belonging to the HQ sample are indicated by single and double plus signs, respectively.

(i) we flag only superposed objects and ribs; (ii) we flag every small fluctuation, including very faint ones at the level of the noise. The resulting profiles are indistinguishable. Further confirmation of the independence of the exact choice of the pixels flagged came from the comparison of independent analysis of the same images (see the next section).

In order to test the sensitivity of our profile to the chosen axis ratio, we compute the profiles of Abell 2218 within elliptical annuli of axis ratios 0.83 and 1. The two profiles are, again, indistinguishable. The profiles of some other clusters, taken from the literature, measured through ellipses of different shapes agree within the errors. Our elliptical profiles do not depend on the adopted axis ratio, because of our selection of the axis length and the fact that the P.A. and ellipticity of the X-ray isophotes are not subject to large variations.

Furthermore, we adjust the background level of the Abell 1656 cluster, the emission of which almost fills the PSPC field of view, in such a way that our profile at large radii matches those derived in literature from the *ROSAT* All-Sky Survey images (Briel, Henry, & Boeringer 1992). Abell 400 exhibits a central point source, a dumbbell galaxy also known as radio source 3C 75, with a slight offset with respect to the center of the cluster emission (cf. Beers et al. 1992). Pixels affected by this source have been flagged. Some other clusters in our list have some peculiar features in their X-ray profile: Abell 1689, 2199, and 2634 present a strong cooling flow (see Allen & Fabian 1998; White, Jones, & Forman 1997; and Schindler & Prieto 1997, respectively). In the following figures, we represent with squares symbols these cooling flow clusters.

3.2. *Comparisons with Previous ROSAT Data*

A comparison between our profiles and those from the literature is quite difficult. For most of the clusters, the data points of the surface brightness profile are not available. Generally, the best-fit parameters for a β-model (Cavaliere & Fusco-Femiano 1976) are the only quantities quoted. We will use these for our comparisons, even if some information is still missing, such as (i) the adopted center, ellipticity, and position angle (for elliptical profiles); (ii) the value of the central brightness; (iii) the radius up to which the data are fitted; and (iv) how well the model describes the profile, in terms of the location of the deviations from the best fit. Finally, some literature values are wrong through mistake or typographical errors.

Figure 2 shows good agreement between the best fits as obtained from literature, once the necessary (if any) correc-

TABLE 2

DATA SET IDENTIFICATION, EXPOSURE TIME, ADOPTED CENTERS, AXIS RATIOS, AND P.A. FOR THE STUDIED CLUSTERS

Name	ID	t_{exp} [a] (s)	Center Coordinates (J2000) R.A.	Decl.	b/a	P.A.[b]
Abell 262	rp800254n00	8163	01 52 47	+36 09 22	0.87	45
Abell 1367	rp800153n00	17610	11 44 49	+19 41 28	1	0
Abell 400	rp800226n00	22203	02 57 35	+06 00 25	0.66	30
Abell 1656	rp800005n00	19819	12 59 42	+27 56 34	1	0
Abell 2199	rp800644n00	38244	16 28 38	+39 32 52	0.76	135
	rp150083n00	10063	16 28 39	+39 33 07	0.76	135
Abell 2634	rp800014a01	9826	23 38 29	+27 01 55	1	0
Abell 2151	rp800517n00	11341	16 04 36	+17 43 21	1	0
Abell 2256	rp100110n00	16452	17 03 54	+78 38 19	1	0
Abell 1904	rp800257n00	3627	14 22 16	+48 30 58	1	0
Abell 401	rp800182n00	6289	02 58 59	+13 34 35	0.6	30
	rp800235n00	7009	02 58 59	+13 34 40	0.6	30
Abell 2670	rp800420n00	16554	23 54 14	−10 24 53	0.74	45
Abell 2218	rp800097n00	39579	16 35 52	+66 12 34	0.83	0
Abell 1689	rp800248n00	13142	13 11 29	−01 20 32	1	0
Abell 520	rp800480n00	4565	04 54 10	+02 55 04	1	0
Abell 963	rp900528n00	9989	10 17 12	+39 02 40	1	0
Abell 223	rp800048n00	6402	01 37 56	−12 49 08	1	0
Abell 222	rp800048n00	6402	01 37 34	−12 59 23	1	0
Abell 2397	rp800344n00	13629	21 56 09	+01 23 25	1	0
Abell 777	rp800049n00	7464	09 29 20	+78 16 34	1	0
Abell 2111	rp800479n00	7028	15 39 41	+34 24 52	1	0
Abell 2125	rp800511n00	11340	15 41 06	+66 16 13	0.6	135
Abell 1758	rp800047n00	16142	13 32 42	+50 32 54	0.7	135
Cl 0024+16	rp800524n00	1069	00 26 35	+17 09 43	1	0
Cl 0939+47	rp800102n00	13098	09 43 00	+46 59 31	0.74	30
Cl 0016+16	rp800253n00	40325	00 18 34	+16 26 16	1	0

NOTE.—The two pointings of Abell 2199 (Abell 401) have been acquired 3 years (6 months) apart. Positions listed assume no pointing errors.

[a] Exposure times are read in the central region of the exposure map.

[b] P.A.s are from north to east counterclockwise.

tions were introduced, and our profiles. Here we note that where we see a local mismatch between the data and the best fit, the same deviations are often observed in the published surface brightness profile.

3.2.1. *Remarks on Individual Clusters*

Abell 262.—David, Jones, & Forman (1996) found that the X-ray isophotes of this cluster twist and ellipticity changes with radius. They present a detailed analysis of the X-ray profile computed through elliptical apertures whose P.A. and ellipticity are fitted to the cluster isophotes. However, they list only counts integrated within ellipses of unspecified P.A. and ellipticity, both of which are probably changing with radius. In our comparison, to compute the surface brightness profile, we calculate the gradient of the integrated flux in each ellipse and make the approximation that it was computed within ellipses with the same center and axis ratio of 0.8. Our profile matches exactly the one from literature at $\log r > 2.4$. The agreement is satisfactory at smaller radii given the approximation involved in the comparison.

Abell 401.—Our points match well those of the Buote & Canizares (1996) β-model. Another observation performed 6 months later is in good agreement with the plotted profile, confirming also the temporal stability of the *ROSAT* PSPC.

Abell 1656.—Our points lie on the best-fit β-models in Buote & Canizares (1996) and Briel et al. (1992).

Abell 2199.—This has been observed twice with a temporal gap of 3 years. As for A401, the two profiles are in good agreement between them and with the Buote & Canizares (1996) β-model.

Abell 2256.—This is a frequently studied merging cluster (Markevitch & Vikhlinin 1997; Buote & Canizares 1996; Briel et al. 1992). Our center is not located on the peak emission but on the barycenter of the X-ray emission. This explains the rising profile at small radii and the slight differences with the fit functions from literature.

Abell 2634.—This cluster presents a strong cooling flow and is not described at all by a β-model for $\log r < 2.4$. At larger radii, where the profile matches the β-model, our data are consistent with the best-fit β-model in Schindler & Prieto (1997).

Cl 0939+4713.—Our profile agrees well with the Schindler & Wambganss (1996) β-profile.

3.3. *Characterization of the Cluster Profiles*

Usually X-ray profiles are characterized through some parameters, resulting from a fit to the data of an appropriate function, generally a β-model. The use of this model presents some problems. First, this method is parametric

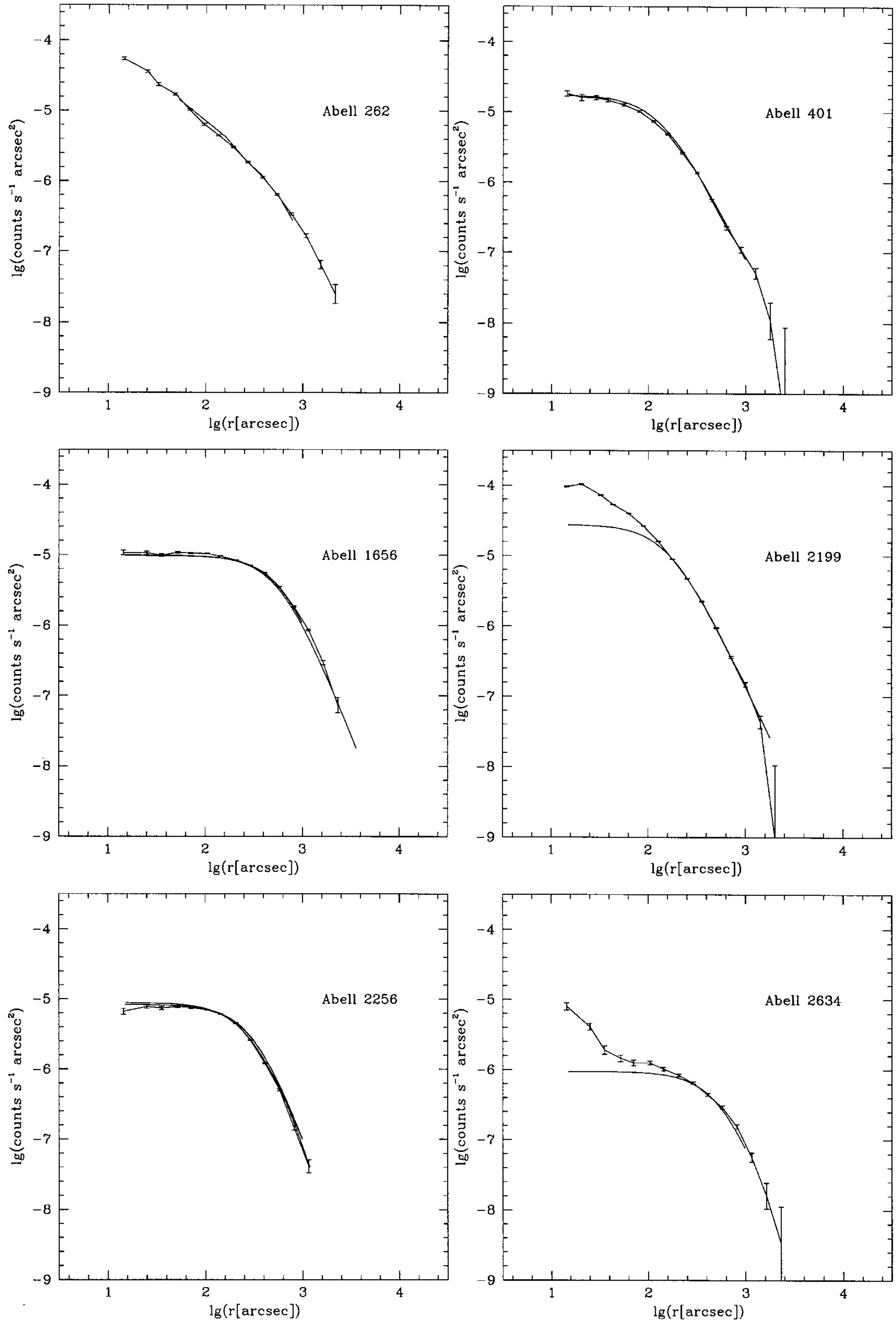

FIG. 2.—Comparison between literature fit and our X-ray profiles

and introduces the width of the bin in the extracted profile as a nonphysical scale. Second, the β-parameter, often referred to as the "slope," is not properly the slope of the profile at large radii, as one can verify calculating the radial gradient of the β-model or, more simply, plotting two profiles with the same β, but different core radii. Third, the best-fit parameters are generally a function of the amplitude of the errors.

For these reasons, we prefer to characterize cluster X-ray profiles through a nonparametric way, computing Pet-

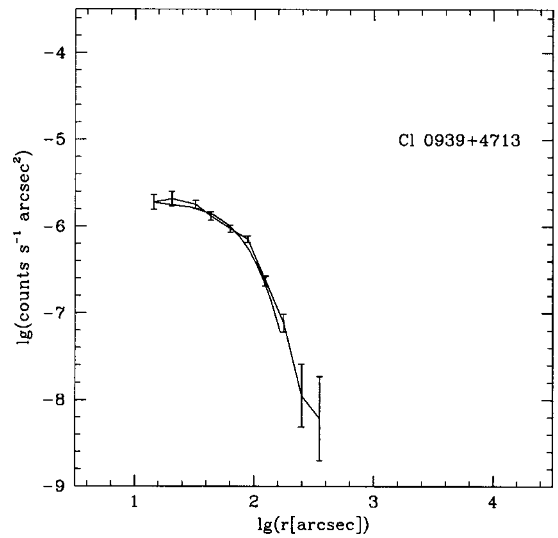

FIG. 2.—*Continued*

rosian (1976) quantities. A detailed and recent presentation of Petrosian quantities can be found in Sandage & Perelmuter (1990). Briefly, the Petrosian radius r_η is defined as the radius where the surface brightness *at* that radius is η times fainter than the surface brightness *inside* that radius. Figure 3 shows the surface brightness [$SB(r)$] and the $\eta(r)$ profiles for a King profile, where $\eta(r) = SB(<r)/SB(r)$.

Choosing a value for η of, say, 2, the corresponding radius $r_{\eta=2}$ is completely determined (in our example $\log r \sim 2.8$). The Petrosian radius, as a ratio between two surface brightnesses, does not depend from quantities that usually affect surface brightnesses, such as Galactic absorption, cosmological dimming, K-correction, and even luminosity evolution if it is the same at all radii. It could be shown (Petrosian 1976), that the Petrosian radius is a metric radius; i.e., its angular dimension is given by the formula relating the physical dimension of a rigid rod and its angular dimension. For objects with profiles of the same shape, the luminosity within a fixed Petrosian radius gives a

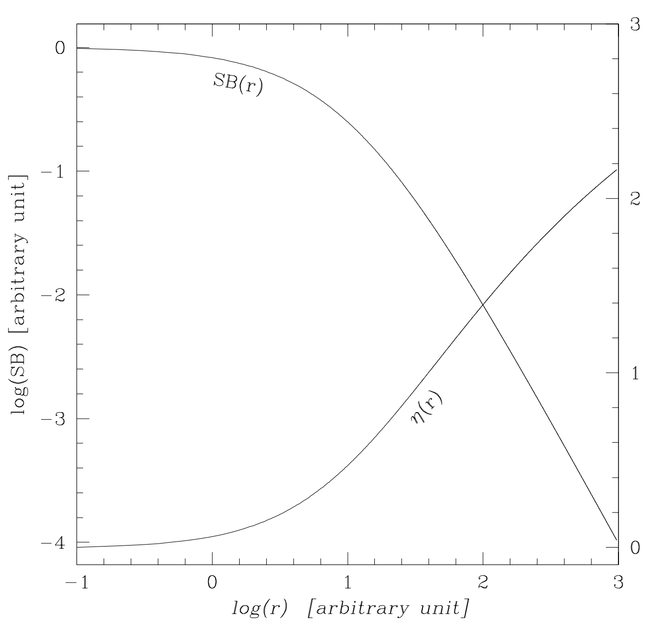

FIG. 3.—SB (surface brightness) and η-profiles for a King profile with $\beta = 0.5$ and arbitrary core radius and central surface brightness.

fixed fraction of the total luminosity, as the effective radius for the de Vaucouleurs's (1948) law. We choose $2.5 \log \eta = 2$, and we refer to it as "$\eta = 2$." For Hubble and β-model (with $\beta = \frac{2}{3}$) profiles, $\eta = 2$ corresponds to 55 and 38 core radii, respectively.

3.4. *Luminosities and Errors*

The count rates have been converted to the flux in the 0.5–2 keV band using a conversion factor of 1.15×10^{-11} ergs s^{-1} cm^{-2}/(counts s^{-1}), almost independent from the gas temperature. The correction for the Galactic absorption has been calculated applying the Morrison & McCammon (1983) model as a foreground absorber to the thermal emission from the intracluster plasma with metallicity fixed to 0.3 (Raymond & Smith 1977; up-to-date version 1992 in XSPEC version 10). Because all clusters are at high Galactic latitude, this correction is small. K-corrections have been computed individually assuming thermal cluster spectrum. Temperatures have been taken from White et al. (1997). For the clusters Abell 222, 223, 777, 963, 1758, 1904, 2125, and Cl 0024+16 and Cl 0939+47, which are not listed in White et al. (1997), we adopt a temperature of 4 keV. Our K-corrections are compatible with the more accurate values plotted by Jones et al. (1998) in their Figure 7. Differences amount to 0.01 in $\log L_X$ at most; i.e., they are negligible.

Our estimate of the uncertainties include Poisson errors and a generous 10% error on the determination of the background level. In Figure 4, and subsequent plots, we do not plot the errors on the X-ray flux, because they are smaller than the symbol size, except for two clusters (Abell 777 and Cl 0024, whose fluxes are lower limits). The median error on $\log L_X$ is 0.015 ergs s^{-1}.

3.5. *Comparison with Data from Previous X-Ray Missions*

For the clusters of our sample, the X-ray luminosities measured by previous missions are listed in various compilations (Soltan & Henry 1983; Lea & Henry 1988; Mushotzky & Scharf 1997; Sadat et al. 1998). Their luminosities are not measured at the Petrosian radii, nor in the *ROSAT* hard band, but are simply aperture or isophotal fluxes, usually in the band of observation. We convert them into our system (flux measured in the Petrosian $r_{\eta=2}$ radius in *ROSAT* hard band) empirically, by means of the median difference between the (log of the) luminosities in common clusters. Our fluxes correlate well with literature data trans-

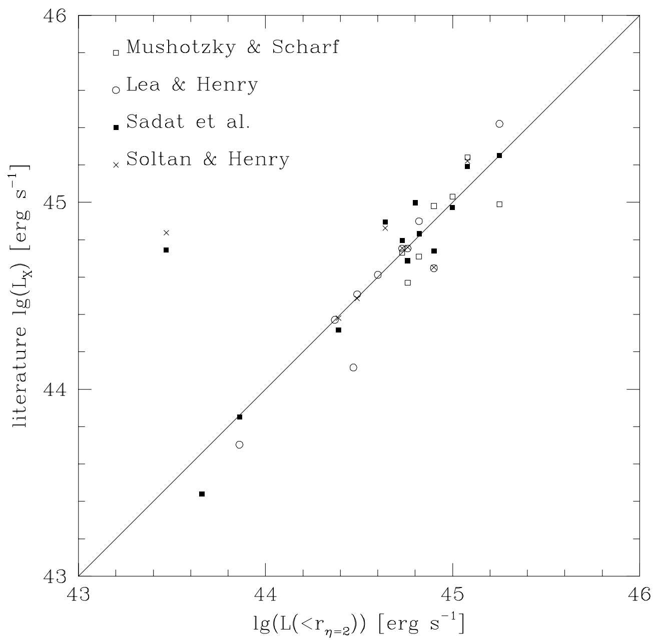

FIG. 4.—Comparison between our metric fluxes in the *ROSAT* hard band and isophotal or aperture fluxes from older satellites converted into our system.

formed in our system, as shown in Figure 4. The large scatter is due to the heterogeneity of literature data and to the transformation from one band to another, because the formal error on the X-ray flux in our system is smaller than the point size. The two outliers refer to the cluster Abell 400, whose central emission has been masked out in our flux measure (see § 3.2.1), but not in the two estimates from literature.

4. RESULTS: THE TRENDS

The aim of this section is to show the existence of trends between quantities related to clusters properties (richness, size, distance, X-ray flux, etc.) and to understand the role played by selection effects on these trends.

4.1. *Size*

Table 3 quotes the $r_{\eta=2}$ size of the HQ sample. All clusters, spanning a large redshift range, from $z \sim 0$ to $z \sim 0.6$, have similar sizes of log $r \sim 3.10$ kpc with a scatter (in log r) of only 0.14 (see Fig. 5). The outliers (at small $r_{\eta=2}$) appear to be cooling flow clusters. Cl 0024+16 and Abell 777 have a too noisy profile to compute $r_{\eta=2}$. Our results confirm those obtained from Henry et al. (1979) and Vikhlinin et al. (1998). Figure 6 shows that clusters have similar size, independently on their X-ray luminosity, at least in the luminosity range sampled (43.5 ergs s^{-1} < log L_X < 45.5 ergs s^{-1}). Furthermore, clusters rich in blue galaxies (Fig. 6, *filled dots*) are not preferentially larger, smaller, brighter, or fainter than those clusters poor in blue galaxies.

Figure 7 compares the optical cluster radius, defined as the radius that encloses 30% of the galaxy population, r_{30}, with our X-ray $r_{\eta=2}$ size, for the HQ sample. The $r_{\eta=2}$ is on average $\sim$3 times larger than r_{30}, with a large scatter. Clusters rich in blue galaxies (*filled dots*) do not have systematically larger or smaller $r_{\eta=2}/r_{30}$ ratios than clusters poor in blue galaxies (*open dots*). Even if the two most distant clusters have both an $r_{\eta=2}/r_{30}$ ratio larger than the average,

TABLE 3

RESULTS OF THE ANALYSIS

Name	log $r_{\eta=2}$ (kpc)	log $L(r < r_{\eta=2})$ (ergs s^{-1})	log $L(r < r_{30})$ (ergs s^{-1})
Abell 262	2.96	43.66	43.64
Abell 1367	3.03	43.86	43.83
Abell 400	3.11	43.47	43.39
Abell 1656	3.10	44.60	44.56
Abell 2199	2.83	44.39	44.41
Abell 2634	3.15	43.78	43.79
Abell 2151	3.33	43.96	43.82
Abell 2256	3.10	44.64	44.62
Abell 1904	3.34	43.86	43.76
Abell 401	3.26	44.80	44.77
Abell 2670	3.03	44.17	44.09
Abell 2218	3.05	44.73	44.75
Abell 1689	2.87	45.08	45.11
Abell 520	3.22	44.90	44.86
Abell 963	3.31	44.82	44.68
Abell 223	3.17	44.47	44.35
Abell 222	3.29	44.49	44.13
Abell 2397	3.12	44.60	44.45
Abell 777	...	~43.86	43.43
Abell 2111	3.24	44.76	44.71
Abell 2125	3.08	44.22	44.14
Abell 1758	3.10	45.00	44.94
Cl 0024+16	...	~44.37	44.25
Cl 0939+47	3.08	44.95	44.41
Cl 0016+16	3.05	45.25	45.07

there is no convincing statistical evidence for a trend of an increasing $r_{\eta=2}/r_{30}$ ratio with redshift.

4.2. L_x *versus* z

Figure 8 shows that in the BO sample there is a deficit of distant clusters with a X-ray luminosity comparable to a faint present-day cluster and an excess of clusters that are as bright as, or brighter than, the brightest nearby clusters. This holds for the HQ sample as well as for the whole sample. The X-ray luminosity is correlated with z at the

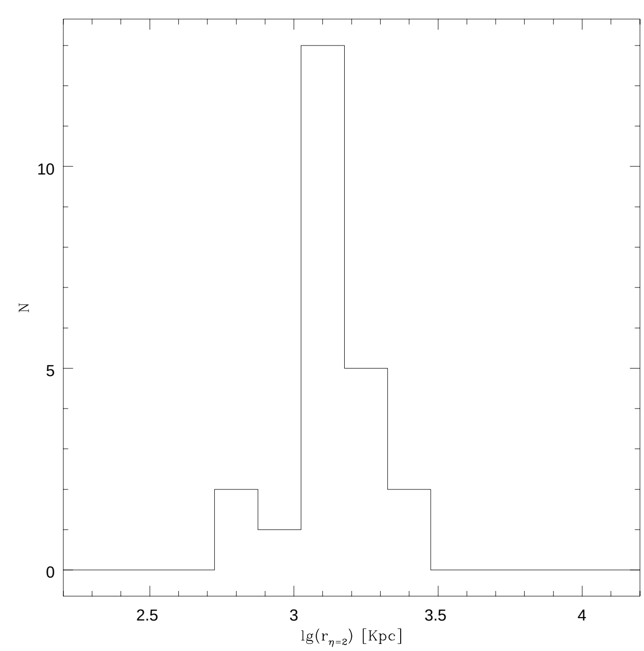

FIG. 5.—Histogram of the $r_{\eta=2}$ sizes of the clusters in the HQ sample

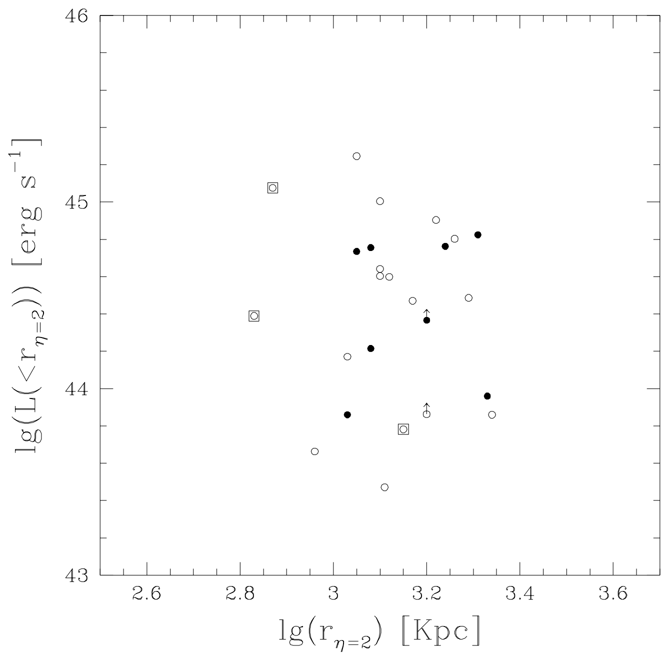

FIG. 6.—X-ray cluster luminosity as a function of the size for clusters in the HQ sample. *Filled dots*, clusters rich in blue galaxies ($f_b > 0.1$); *open dots*, clusters poor in blue galaxies; *squares*, cooling flow clusters.

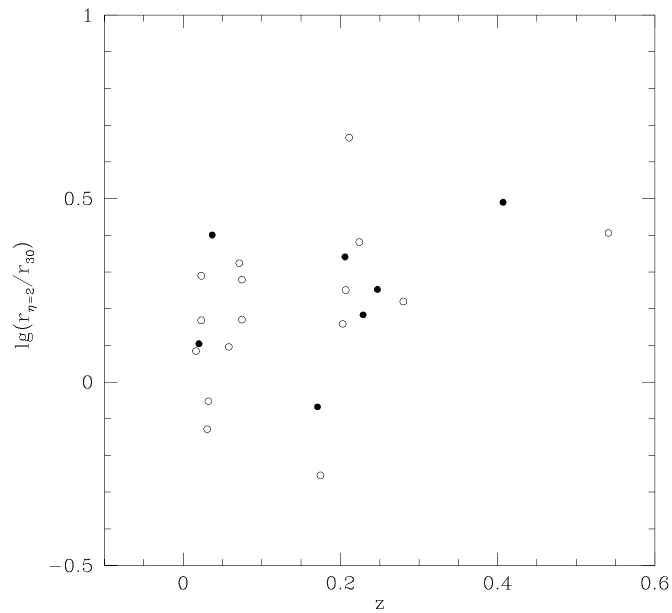

FIG. 7.—Ratio between the optical radius r_{30} and the X-ray size $r_{\eta=2}$ as a function of z for clusters in the HQ sample. Symbols as in Fig. 6.

99.9% confidence level, according to the Spearman r_s and Kendall τ-tests. The X-ray luminosity of the four clusters not present in the HQ sample has been converted to our energy band as described in § 3.5. In the whole sample, clusters rich in blue galaxies (*filled dots*) are not preferentially the brightest or the faintest ones. The correlation between X-ray luminosity and redshift is still present if we use r_{30} or a 3 Mpc aperture for all clusters. If we remove the irregular clusters identified by Butcher & Oemler (1984) from the sample, the correlation is still present, but only at the 98.5% confidence level.

In the X-ray waveband, distant clusters are not brighter in the past than today, and, if anything, they were fainter in the past, not brighter (Henry et al. 1992; Collins 1997; Vikhlinin et al. 1998; Rosati et al. 1998). On the other hand, the X-ray luminosity of the clusters in the BO sample, which span the same redshift and luminosity range of the abovementioned *representative* samples, increases with redshift (or low-luminosity clusters are missing at large z in the sample). This means that the BO sample is not representative of a homogeneous class of clusters of galaxies observed at different look-back times, but it is biased toward an increasing fraction of bright X-ray clusters as the redshift increases. We postpone the discussion of the relevance of the trend in the BO effect to the next section.

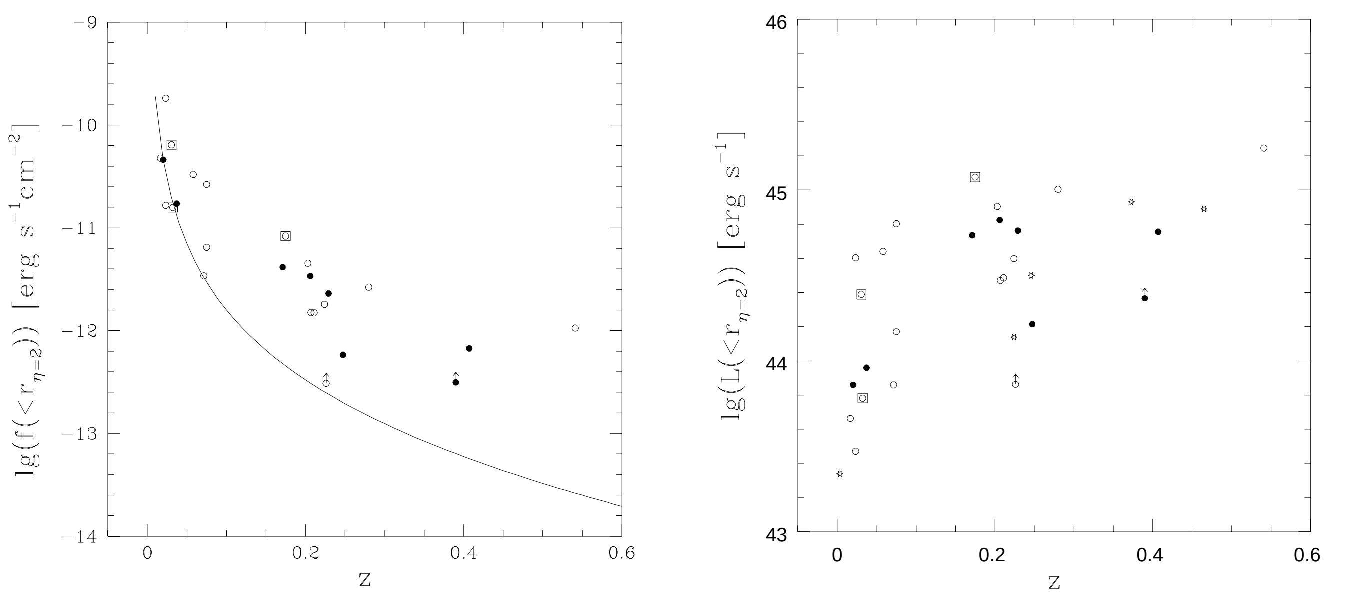

FIG. 8.—X-ray luminosity as a function of z. *Left panel*: Apparent flux of clusters in the HQ sample. The curve is the locus of the clusters having an X-ray emission 5 times smaller than Abell 1656 (Coma), assuming a K-correction equal to zero. Points are not corrected for absorption or K-correction. *Right panel*: Absolute luminosity for the whole sample. Absorption and K-corrections have been applied to the data. Literature data are plotted as star points. Other symbols as in Fig. 6.

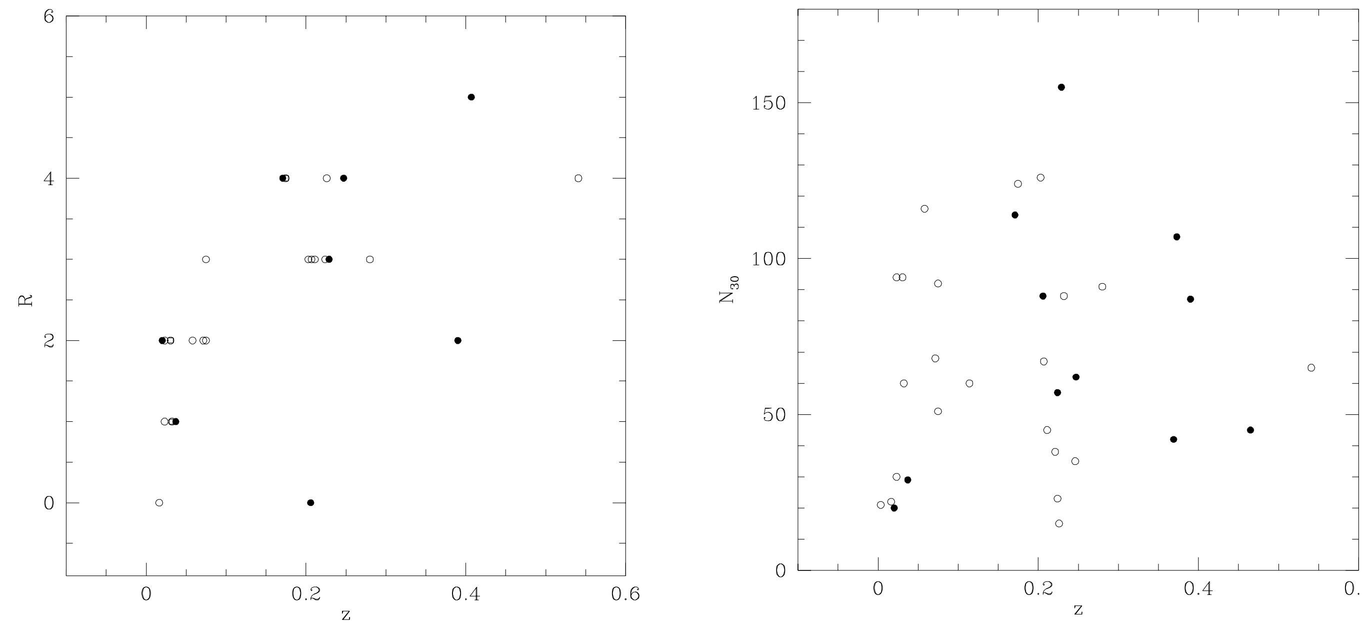

FIG. 9.—Richness as a function of z for the whole sample. *Left panel*: ACO richness. *Right panel*: BO richness. *Filled dots*, clusters rich in blue galaxies ($f_b > 0.1$); *open dots*, clusters poor in blue galaxies.

The existence of a strong correlation between X-ray luminosity and redshift, in the BO sample, makes suspicious any other correlation involving these two quantities.

4.3. *Richness versus z*

In hierarchical scenarios, clusters at high redshift are more massive, on average, than nearby clusters, because only the richest clusters are already formed. Instead, the ancestors of present-day clusters were less massive than today, and they had not yet formed at high redshift. Therefore, it is expected that at higher redshift, clusters (which have already formed) are richer than nearby ones.

Figure 9 shows that the distant clusters in our sample are also the ones with higher ACO richness. The Spearman r_s and Kendall τ-tests reject ($>99.9\%$ confidence level) that the richness is not correlated with z. Dressler et al. (1997), in their study of the morphological segregation in clusters at $z \sim 0.4$ (half of these taken from the BO list), noted that the distant clusters are denser than nearby ones listed in Dressler (1980).

The increase of the cluster richness with redshift in our (BO) sample is not due to the evolution of clusters, but to just two selection effects: richness and X-ray luminosity (see Fig. 10), and X-ray luminosity and redshift (see Fig. 8), are

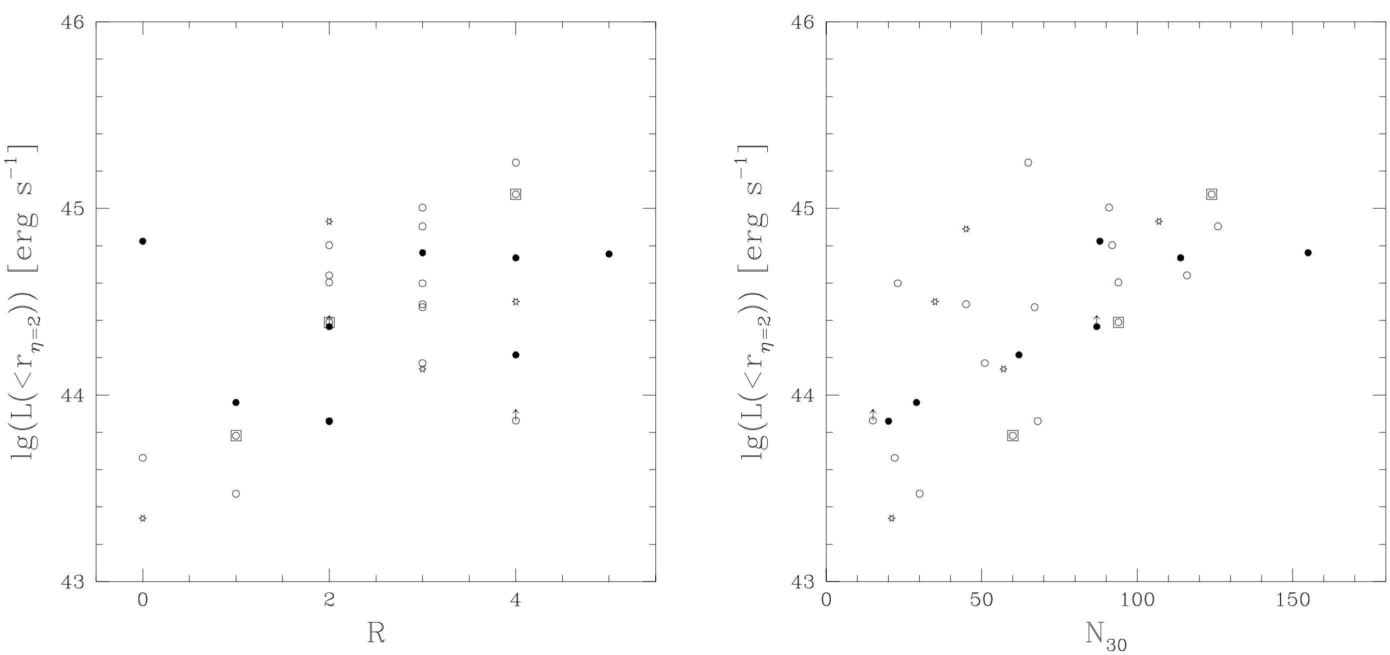

FIG. 10.—X-ray luminosity as a function of the cluster richness for the whole sample. *Left panel*: ACO richness. *Right panel*: BO richness. Symbols as in Fig. 8.

correlated. The latter correlation is certainly a bias, and this induces a correlation between redshift and richness. Therefore, the trend between richness and redshift is not a property of the clusters but a result of the (poorly known) selection criteria adopted for assembling the sample.

The (apparent) evolution of the cluster richness is easy to understand from an observational point of view. In the optical, clusters are usually detected as galaxy overdensity over the field. As the redshift increases, the clusters have to be richer and richer to be detected, and distant poor clusters are likely to be missing in all optically selected catalogs. The ACO catalog, on which the Butcher-Oemler sample is largely based (note also that Cl 0939+47 is listed in the ACO catalog as Abell 851), is complete up to $z \sim 0.1$ (Scaramella et al. 1991). At larger redshifts only the richest clusters are present, whereas at small redshift the number of very rich clusters is small because of the small local volume.

The right panel of Figure 9 shows that the central richness, N_{30}, of clusters with PSPC data does not increase with redshift, contrary to that expected from its correlation with X-ray luminosity (Fig. 10) and from the increase of the X-ray luminosity with z (Fig. 8). However, it is quite dangerous to do predictions by propagating correlations between quantities, especially in a biased sample such as ours, because too many properties are changing at the same time as the redshift varies.

N_{30} and R do not show any statistically significant correlation (the Spearman test indicates a correlation at the 60% confidence level). Poor clusters, in the ACO sense, do not have too many galaxies within R_{30}, whereas rich clusters can be very rich, as well as very poor, in the center. This means that clusters have a variety of galaxy density profiles for a given N_{30} or R, since for the same total number of bright galaxies, R, they can have a quite different central number of galaxies, N_{30} (and vice versa). Alternatively, large observational errors affect these two quantities.

4.4. L_x *versus Richness*

Figure 10 shows that in the whole sample the cluster X-ray luminosity increases with galaxy richness, as measured by either Abell et al. (1989) or Butcher & Oemler (1984). Clusters that are rich in blue galaxies (*filled dots*) span the entire range explored in richness and luminosity. The correlation between X-ray luminosity and cluster richness is expected (see, e.g., Bahcall 1974; Jones & Forman 1978). However, in our sample, this correlation is probably the result of two selection effects: as the redshift increases, we sample (i) brighter (see Fig. 8) and (ii) richer (Fig. 9, *left panel*) clusters. Our statement can be checked using the data from Smail et al. (1998), who studied very bright X-ray–selected clusters, independently from their optical richness. Their clusters have log $L_x \sim 45$ ergs s^{-1}, $0 < R < 3$, and $15 < N_{30} < 60$. Adding these data to ours, the correlation between richness and X-ray luminosity largely disappears, thus confirming that the found correlation is the result of the selection criteria instead of a real cluster property (Fig. 11).

4.5. L_x *versus* f_b

A correlation between L_x and f_b would explain many cluster properties. The lack of blue galaxies in the cluster core, the color distribution of spiral galaxies, and many of their properties, such as velocity and position relative to the cluster center, higher surface brightness (Andreon 1996), and H I deficiency of infalling spirals (Gavazzi 1987), can be explained if spirals falling in clusters have a starburst due to the ram pressure in the hot gas (Bothun & Dressler 1986) that consumes the galaxy's gas reservoir. During the burst, these galaxies become bluer and brighter in the mean surface brightness. Just after the burst, they become as red as elliptical galaxies (Charlot & Silk 1994), explaining the presence of red spiral galaxies in cluster cores. Furthermore,

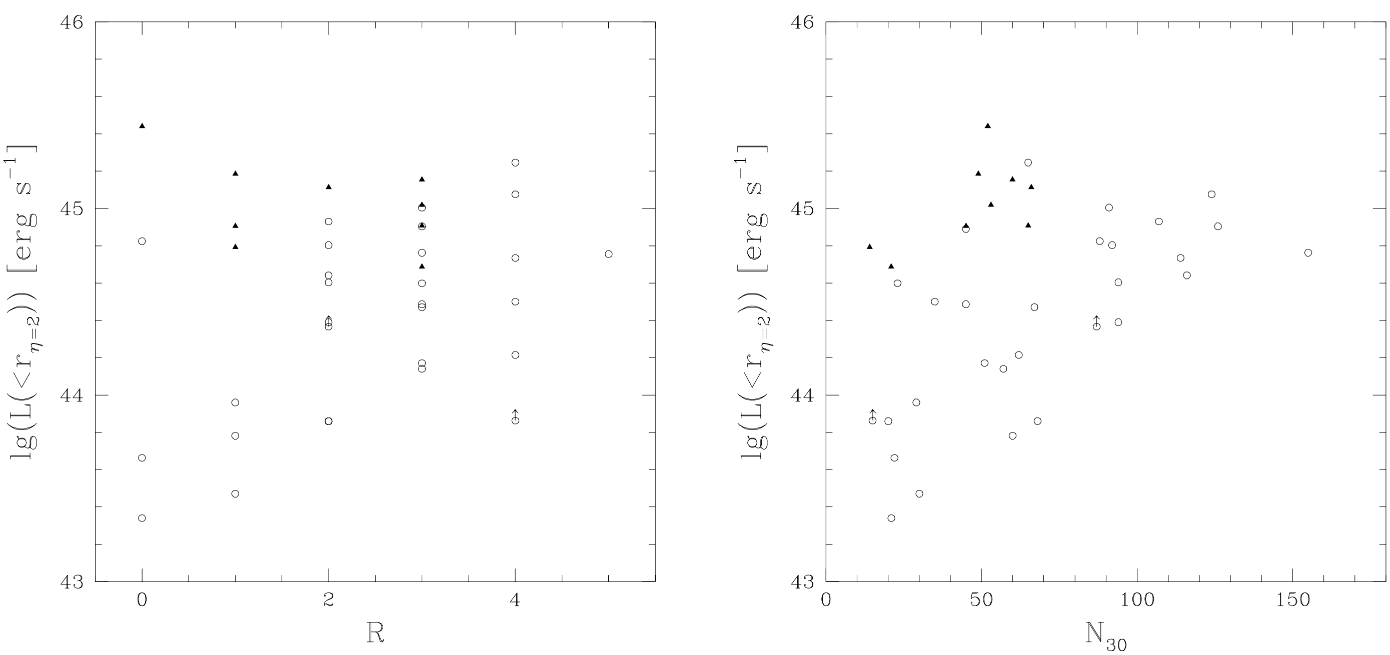

FIG. 11.—X-ray luminosity as a function of the cluster richness, including the Smail et al. (1998) sample. *Left panel*: ACO richness. *Right panel*: BO richness. *Open dots*, the optically selected BO sample; *filled triangles*, the X-ray–selected sample.

both the existence of galaxies that show spectral signatures consistent with the presence of intermediate-age stellar populations (Couch & Sharples 1987; Lavery & Henry 1988; Dressler & Gunn 1992) and the photometric evidence for the blue starburst spirals in Coma (Donas, Milliard, & Laget 1995; Andreon 1996) give support to this scenario.

We do not observe any correlation between X-ray luminosity and the fraction of blue galaxies for the whole sample and for the HQ sample. In a sample of 10 clusters at moderate redshift ($z \sim 0.25$), which spans just a factor of 2–3 in X-ray luminosity, a wide spread is found in the fraction of blue galaxies (Smail et al. 1998), which is uncorrelated to X-ray luminosity. Using *Einstein Observatory* data, Lea & Henry (1988) suggest the possible existence of a correlation between these two quantities in a subsample of the BO list, provided that deviant points (low-luminosity clusters and the most distant cluster) are discarded. The absence of a correlation between the fraction of blue galaxies and the cluster X-ray luminosity implies that this link, if it exists, is complex and needs more physical parameters to be explained than only the spiral fraction and the X-ray luminosity.

Here we note that these quantities are not averaged on the same cluster area, nor on regions whose area ratio is fixed: sometimes the optical radius is 3 times larger than the area over which the spiral fraction has been computed, and sometimes it is 2 times smaller (see Fig. 7). For these reasons, we have recalculated the cluster X-ray luminosities within the radius r_{30} used for computing the cluster spiral fraction, but still any significant correlation between these two quantities does not appear.

5. RELEVANCE OF THESE TRENDS IN THE CONTEXT OF THE BO EFFECT

Any sample of local and distant clusters that is not statistically complete can be affected by the selection criteria adopted to assemble it. This happens because (i) clusters have morphological differences in the nearby universe (Zwicky 1957) and at $z \sim 0.4$ (Oemler et al. 1998) and (ii) their galaxy populations are subjected to several segregation effects, in galaxy morphology (Hubble & Humason 1922; Dressler 1980; Sanromà & Salvador-Solé 1990; Whitmore, Gilmore, & Jones 1993; Andreon 1994, 1996; Dressler et al. 1997; Andreon et al. 1997), color (Butcher & Oemler 1984; Mellier et al. 1988; Donas et al. 1995; Andreon 1996), and spectral properties (Biviano et al. 1997 and references therein).

In particular, any selection done on the basis of the richness is contaminated by several factors, such as our ignorance of the physical evolution of the cluster richness or the role played by local phenomena as the enhancement in brightness due to starburst activity. In this sense, selecting clusters according to their X-ray luminosity is safer, because the physics of the X-ray emission is well known and is easier to detect (the X-ray emission goes as the square of the density, instead of the density for optical richness). Once a sample of clusters is properly defined, the assumption made is that the same class of objects are compared at different look-back times.

Our results show that the main cluster sample studied up to now in the context of the BO effect is biased: the X-ray luminosity of these clusters increases with the redshift, contrary to the recent observational evidence for representative samples (see § 4.2). Thus, the nearby and distant clusters in the BO sample are not representative of a fair sample. This implies that any trend highlighted in the BO sample could be the product of the selection criteria adopted instead of real differences with respect to the age of the systems.

Differences in X-ray luminosity reflect, to a large extent, differences in the intracluster gas temperature and gas density and, consequently, in the cluster mass (Quintana & Melnick 1982; Edge & Steward 1991; White et al. 1997). Oemler et al. (1997) supposed that they were studying richer and richer clusters as the redshift increases and that distant clusters were growing in a way different from present-day clusters, i.e., merging smaller clumps at a higher rate, as hierarchical scenarios suggest (Kauffmann 1995). This conclusion supposes a physical evolution of the clusters in the BO sample, whereas instead the richness of the clusters in the BO list increases just because of selection effects.

Another piece of evidence for the presence of a selection bias in the BO sample comes from the fact that the BO effect is only evident in optically selected cluster samples. In fact, clusters selected in the X-ray band, with almost the same X-ray luminosity and $z \sim 0.25$, show blue fraction values with a large range and with a mean similar to that observed in nearby clusters (Smail et al. 1998). This mean value is also smaller than the blue fraction in the BO clusters at the same redshift.

To summarize, the BO sample does not contain the same class of objects at different look-back times, contrary to the requirement to detect any sign of evolution in a sample.

We note that, although this bias affects the BO sample, it could not lower the significance of the BO effect, if X-ray bright clusters have the same blue fraction of much fainter clusters. This is a hypothesis that, at the present time, we cannot test observationally on an unbiased sample. In the BO biased sample, the fraction of blue galaxies does not seem to depend on the X-ray cluster properties. Furthermore, the BO effect is evident even after removing the faint clusters with $\log L_X < 44$ ergs s^{-1} and $z < 0.1$. However, we do not know if this reduced sample (or any other subsample drawn from the BO sample) is representative for the range of redshift studied, and any conclusion drawn from it should be regarded with caution. In conclusion, we do not believe that selection biases are completely removed by eliminating offending clusters.

From the theoretical point of view, Kauffmann (1995) shows that in their model of cluster formation and evolution the fraction of blue galaxies does not depend on the cluster mass, at least for rich clusters. In that case, there is no risk in comparing clusters of different masses (X-ray luminosities) at different redshift for studying the BO effect. We stress, however, that the evolutionary interpretation of the BO effect still holds only under the hypothesis that these selection biases do not affect the sample, a hypothesis that must be shown to be true.

Galaxies in groups do not show the BO effect (Allington-Smith et al. 1993) over the same redshift range. For this reason, and under the assumption of the evolutionary interpretation of the BO effect in clusters, Allington-Smith et al. (1993) claim that evolution is driven by environment much more than look-back time. However, selection criteria of studied groups and clusters are quite different: groups are *not* optically selected, because Allington-Smith et al. (1993) built their group sample by selecting the galaxies around radio galaxies of a given radio flux, which is likely to be uncorrelated with the optical luminosity of the galaxy hosting the radio source or with the group optical properties. Instead, the BO cluster sample is biased toward very rich (and X-ray luminous) clusters at high redshift. We think that the claim of a differential evolution of galaxies in clusters compared to those in groups, should wait on a proper determination of the amplitude of the BO effect in a sample of clusters representative of their redshift.

6. CONCLUSIONS

We have analyzed *ROSAT* PSPC images of most of the clusters studied in relation to the Butcher-Oemler effect. We have computed surface brightness profiles, as well as X-ray fluxes within metric diameters adapted to the cluster size (Table 3). Our main results are the following:

1. The cluster X-ray size, as measured by the Petrosian $r_{\eta=2}$ radius, does not evolve and is independent of X-ray luminosity: log $r_{\eta=2} \sim 3.10 \pm 0.14$ kpc.

2. The X-ray luminosity of clusters listed in the Butcher-Oemler sample increases with redshift (Fig. 8). In the same redshift range, there is observational evidence, from *representative* samples, that the X-ray luminosity of clusters is constant or decreasing i.e., had a trend opposite to those observed in BO sample. Therefore, nearby and distant clusters in the BO sample are not representative of a given class of objects observed at different epochs, and thus the BO sample does not contain the same class of objects at different look-back times, contrary to the requirement to detect any sign of evolution in a sample.

Because selection criteria modify the sample composition in a redshift-dependent way, it is quite difficult to disentangle a real redshift dependence (evolution) from a fictitious redshift trend induced by selection criteria. Hence, the observed BO effect measured from optically selected samples is *not necessarily* a general property of clusters of galaxies, but could be a selection effect. There is some independent support for this interpretation: it seems that X-ray–selected clusters, all of similar X-ray luminosity and therefore likely to belong to the same class, do not show the BO effect (Smail et al. 1998). Similarly, galaxies in radio-selected groups show no evolution, besides a passive one (Allington-Smith et al. 1993).

The variety of optical shapes and sizes of clusters, together with the Malmquist-like bias and the incompleteness of the BO list, are the main sources for the trends present in the sample.

X-ray data have been of fundamental importance in revealing the existence of a selection bias that mimics the trend usually interpreted as evidence of evolution. It is not surprising, therefore, that our conclusions differ from those reached when X-ray data were not available.

3. The ACO richness of clusters listed in the Butcher-Oemler sample increases with redshift. We interpret this correlation as an observational effect: poor clusters are scarcely detected at high redshift, and, unusually, rich clusters are missing in low-redshift samples. Other cluster quantities (N_{30}, L_X, etc.) shows some correlation among them or with redshift. We explain these as the effect of selection criteria. Adding to our sample a sample of X-ray–selected clusters, the correlations generally lose strength, suggesting the correctness of our interpretation.

4. The usual interpretation of the BO effect, as due to evolution, holds only assuming that selection effects have not practical relevance, a hypothesis that must be tested. The absence of correlation between the fraction of blue galaxies and the X-ray luminosity of the clusters may suggest such a possibility.

We are grateful to Sabrina de Grandi for her support and availability at the beginning of this work and to David White and Gilles Theureau for their suggestions on the manuscript. Constructive comments by D. Burstein, G. Bothun, and an anonymous referee improved this paper. S. E. acknowledges M. Capaccioli for the financial support of the publication charges of this paper. S. A. dedicates this work to his grandfather, Ismaele Andreon, recently deceased.

REFERENCES

Abell, G., Corwin, H., & Olowin, R. 1989, ApJS, 70, 1
Allen, S., & Fabian, A. 1998, MNRAS, 297, L57
Allington-Smith, J., Ellis, R., Zirbel, E., & Oemler, A. 1993, ApJ, 404, 521
Andreon, S. 1994, A&A, 284, 801
———. 1996, A&A, 314, 763
Andreon, S., Davoust, E., & Heim, T. 1997, A&A, 323, 337
Bahcall, N. 1974, ApJ, 193, 529
Beers, T. C., Gebhardt, K., Huchra, J. P., Forman, W., Jones, C., & Bothun, G. D. 1992, ApJ, 400, 410
Biviano, A., Katgert, P., & Mazure, A., Moles, M., Den Hartog, R., Perea, J., & Focardi, P. 1997, A&A, 321, 84
Bothun, G., & Dressler, A. 1986, ApJ, 301, 57
Briel, U., Henry, J., & Boeringer, H. 1992, A&A, 259, L31
Buote, D., & Canizares, C. 1996, ApJ, 457, 565
Butcher, H., & Oemler, A. 1977, ApJ, 219, 18
———. 1984, ApJ, 285, 426
Cavaliere, A., & Fusco-Femiano, R. 1976, A&A, 19, 137
Charlot, S., & Silk, J. 1994, ApJ, 432, 453
Collins, C., Burke, D., Romer, A., Sharples, R., & Nicol, R. 1997, ApJ, 479, L117
Couch, W., & Sharples, R. 1987, MNRAS, 229, 423
David, L., Jones, C., & Forman, W. 1996, ApJ, 473, 692
de Vaucouleurs, G. 1948, Ann. d'Astrophys., 11, 247
Donas, J., Milliard, B., & Laget, M. 1995, A&A, 303, 661
Dressler, A. 1980, ApJ, 236, 351
Dressler, A., & Gunn, J. 1992, ApJS, 78, 1
Dressler, A., et al. 1997, ApJ, 490, 577
Edge, A., & Stewart, G. 1991, MNRAS, 252, 428
Ellis, R., Smail, I., Dressler, A., Couch, W., Oemler, A., Butcher, H., & Sharples, R. 1997, ApJ, 483, 582
Gavazzi, G. 1987, ApJ, 320, 96
Jones, C., & Forman, W. 1978, ApJ, 224, 1
Jones, L., Scharf, C., Ebeling, H., Perlman, E., Wegner, G., Malkan, M., & Horner, D. 1998, ApJ, 495, 100
Henry, J., Branduardi, G., Fabricant, D., Feigelson, E., Murray, S., Tananbaum, H., Briel, U., & Soltan, A. 1979, ApJ, 234, L15
Henry, J., Gioia, I., Maccacaro, T., Morris, S. L., Stocke, J. T., & Wolter, A. 1992, ApJ, 386, 408
Hubble, E., & Humason, M. 1926, ApJ, 64, 321
Kauffmann, G. 1995, MNRAS, 274, 161
Koo, D. 1981, ApJ, 251, L75
Lavery, R., & Henry, J. P. 1988, ApJ, 330, 596
Lea, S. M., & Henry, J. P. 1988, ApJ, 332, 81
Markevitch, M., & Vikhlinin, A. 1997, ApJ, 491, 467
Mellier, Y., Soucail, G., Fort, B., & Mathez, G. 1988, A&A, 199, 13
Morrison, R., & McCammon, D. 1983, ApJ, 270,119
Mushotzky, R., & Scharf, C. 1997, ApJ, 482, 13
Oemler, A., Dressler, A., & Butcher, H. 1997, ApJ, 474, 561
Petrosian, V. 1976, ApJ, 209, L1
Quintana, H., & Melnick, J. 1982, AJ, 87, 972
Rakos, K., & Schombert, J. ApJ, 439, 47
Raymond, J. C., & Smith, B. W. 1977, ApJS, 35, 419
Rosati, P., Della Ceca, R., Norman, C., & Giacconi, R. 1998, ApJ, 492, L21
Sadat, R., Blanchard, A., Guiderdoni, B., & Silk, J. 1998, A&A, 331, L69
Sandage, A. 1988, ARA&A, 26, 561
Sandage, A., & Perelmuter, J.,-M. 1990, ApJ, 350, 481

Sanromà, M., & Salvador-Solé, E. 1990, ApJ, 360, 16
Scaramella, R., Zamorani, G., Vettolani, G., & Chincarini, G. 1991, AJ, 101, 342
Schindler, S., & Prieto, M. 1997, A&A, 327, 37
Schindler, S., & Wambganss, J. 1996, A&A, 313, 113
Smail, I., Edge, A., Ellis, R., & Blandford, R. 1998, MNRAS, 293, 124
Soltan, A., & Henry, J. 1983, ApJ, 271, 442
Stanford, S., Eisenhardt, P., & Dickinson, M. 1998, ApJ, 492, 461
Stark, A., Gammie, C., Wilson, R., Bally, J., Linke, R. A., Heiles, C., & Hurwitz, M. 1992, ApJS, 79, 77
Vikhlinin, A., McNamara, B., Forman, W., Jones, C., & Quintana, H. 1998, ApJ, 498, L21
White, D. A., Jones, C., & Forman, W. 1997, MNRAS, 292, 419
Whitmore, B., Gilmore, D., & Jones, C. 1993, ApJ, 407, 489
Zwicky, F. 1957, Morphological Astronomy (Berlin: Springer)